Dynamical string-parton model for relativistic heavy-ion collisions

D. J. Dean,[1,2,3] A. S. Umar,[1,2] J.-S. Wu,[1,2] and M. R. Strayer[1,2]
[1] *Center for Computationally Intensive Physics, Physics Division, Oak Ridge National Laboratory, Oak Ridge, Tennessee 37831*
[2] *Physics Division, Oak Ridge National Laboratory, Oak Ridge, Tennessee 37831*
[3] *Vanderbilt University, Department of Physics & Astronomy, Nashville, Tennessee 37235*
(Received 11 July 1991)

We introduce a dynamical model for the description of hadron-hadron collisions at relativistic energies. The model is based on classical Nambu-Gotō strings. The string motion is performed in unrestricted four-dimensional space-time. The string end points are interpreted as partons which carry energy and momentum. We study e^+e^-, e-p, and p-p collisions at various center-of-mass energies. The three basic features of our model are as follows. An ensemble of strings with different end-point dynamics is used to approximately reproduce the valence quark structure functions. We introduce an adiabatic hadronization mechanism for string breakup via $q\bar{q}$ pair production. The interaction between strings is formulated in terms of a quark-quark scattering amplitude and exchange.

PACS number(s): 25.70.Np, 24.10.–i, 12.40.Aa

I. INTRODUCTION

It has been suggested that collisions of heavy ions at relativistic energies may achieve high enough temperatures and energy densities to induce a phase transition from an ordinary hadronic matter to a new and novel form of matter called the quark-gluon plasma [1]. This form of matter may have been formed during the first few moments of the Universe and it is of significant importance for cosmological studies. Presently, there is no convincing evidence that this state of matter has been achieved in the laboratory. However, it is believed that the conditions for the formation of the plasma will be attainable at the Relativistic Heavy-Ion Collider (RHIC) facility, under construction at the Brookhaven National Laboratory. Detection of the plasma formation also poses difficult experimental and theoretical questions. At the moment there is no clear hadronic signal suggesting the formation of the plasma. The difficulty is mostly due to the confining nature of the strong interaction, which only allows hadronic final states, and thus a detailed understanding of all of the hadronic decay processes is necessary before the identification of the plasma can be achieved.

A rigorous theoretical understanding of the quark-gluon plasma and its formation is, in principle, given by quantum chromodynamics (QCD). The physics of relativistic heavy-ion collisions encompasses both perturbative and nonperturbative aspects of QCD. While lattice gauge theory calculations [2] have shown the confining nature of QCD, application to the study of strong-interaction dynamics of hadronic collisions including the hadronization process is in its infancy. A number of finite-temperature lattice gauge calculations, including dynamical fermions, have been performed to determine the nature of the phase transition to the quark-gluon plasma [3] and to study the properties of the plasma [4]. Earlier calculations on coarse lattices suggested a first-order chiral phase transition from hadronic to quark matter [3]. However, recent refined calculations with two and three dynamical quarks seem to question such a phase transition [5] for realistic quark masses. In the absence of a real-time dynamical theory for hadronic processes, it is desirable to develop an effective formalism which includes at the onset some of the important properties dictated by QCD and makes a connection with the successful models of the strong-interaction physics such as the quark-parton model and its dynamical extensions [6–8]. The parton model largely relies on the property that QCD displays asymptotic freedom at large momentum transfer where this high-energy QCD phenomenology is believed to be valid. In this sense the parton model may be applicable during the early stages of the relativistic heavy-ion collisions where the constituent quarks are expected to interact in a way consistent with the assumptions of this phenomenology [9]. The later stages of the reaction are governed by the strongly dynamical and nonperturbative aspects of QCD and requires a different treatment.

In this paper we introduce a real-time dynamical model for studying the inclusive properties of hadronic collisions. The model is based on the Nambu-Gotō string description of hadrons supplemented by extensions to incorporate the basic features of the parton model, together with a hadronization mechanism. The relativistic covariant string model of hadrons was born from attempts to construct a dual crossing symmetric Regge theory of hadronic interactions [10]. The string action, being proportional to the invariant area swept by the string, results in a linear confining potential in a way similar to the area dependence of the Wilson loop parameter in the high-temperature limit of the Euclidian lattice QCD. In the string picture the quarks are attached at the ends

of a string at all times and the confinement is an integral part of the model. The Nambu-Gotō strings produce linearly rising Regge trajectories for the hadronic spectrum and reproduce the masses of hadronic resonances [10]. Although a precise connection between QCD and the string theory is not established, lattice QCD calculations for heavy quarks at finite separation [11] and dual long-distance QCD studies [12] suggest stringlike solutions in the large number of flavors limit. Similarly, the inclusion of the gluonic degrees of freedom into the quark model via the strong-coupling Hamiltonian lattice formulation of QCD [13] has shown promise in performing nonperturbative calculations of hadron properties and even the calculation of meson-meson interactions [14, 15]. In this approach the gluon degrees of freedom condense into a collective "stringlike" object called the flux tube. The flux tube describes the gluon dynamics at appreciable quark separations. It has also been suggested that a giant flux tube may be formed between two receding heavy ions due to the stochastic exchange of soft gluons between the constituent quarks of the two nuclei [16]. This giant flux tube of color plasma is believed to be formed by a large number of strings coalescing in a small volume [17]. It would be interesting to determine whether such high string densities are attainable through a dynamical string description of heavy-ion collisions. However, relativistic strings do not contain the transverse excitation modes available in ordinary flux tubes. On the other hand, as we will show below, it is possible to use an ensemble of strings with different endpoint dynamics to obtain a good description of the parton structure functions. This is an important development in making a connection between relativistic strings and the parton model.

The real-time dynamics of boosted strings must be supplemented by a hadronization mechanism and an interaction mechanism. For the hadronization mechanism we use the pair creation followed by a string breakup method which is similar to flux-tube breaking of the strong-coupled QCD calculations [18]. Some experimental evidence may also be provided by the studies of jets in e^+e^- and p-p collisions. These experiments demonstrate that jets originate from hard quarks and gluons and provide support that fragmentation takes place within color neutral systems and not from isolated partons [19]. This decay procedure will be extended to take into account a decay time between the formation of the off-mass-shell $q\bar{q}$ pair, and the final hadronic production. Our procedure is consistent with the inside-outside cascade picture observed in relativistic collisions.

Introduction of string-string interactions has always been the more difficult aspect of dynamical calculations [20, 21]. The well known arm-exchange mechanism for string interactions provides about 1.5 mb of the total 30 mb inelastic p-p cross section. One solution for this deficiency has been the assumption of a "flux-tube radius" for the strings [20]. However, even with this nonlocal interaction mechanism the transverse motion remains minimal and grossly underestimates the transverse momentum distributions. In the realm of the parton model this is partially due to the inability of the string phenomenology to incorporate parton-parton collisions. Such hard collisions are believed to be a major source of large transverse momentum production both in hadron-hadron [22] and in relativistic heavy-ion [23, 24] collisions.

The primary focus of our approach to the string-string interactions are the string end points which are interpreted as dynamical quarks. The quarks on each string act as distinguishable particles [14] and scatter with a phenomenological amplitude. This interaction is followed by the exchange of the two quarks in analogy with quark-exchange mechanisms mentioned elsewhere [25, 26]. The dynamics of boosted relativistic strings lead to a distribution of particles with a rapidity plateau, and with the initial quarks producing leading particle effects [27]. The result is a dynamical model with relatively few free parameters which could be applied to the study of relativistic heavy-ion collisions. The parameters of the model are fixed by comparing to e^+e^-, e-p, and p-p collisions. We also note that the real-time string-parton model is considerably different from other string-based statistical models [28, 19]. The string-based fragmentation models include the LUND model [28], which is initialized by a QCD-based parton distribution and then allowed to hadronize via a prescribed fragmentation scheme. The extension of the LUND model, FRITIOF [29], assumes that excited hadrons behave like a chain of color dipoles which move like relativistic strings. Interactions are introduced via multiple small momentum exchanges between the color dipoles of two overlapping strings. Other nondynamical models are the dual-parton model [30], in which the strings are formed by a soft gluon exchange between the valence partons of the colliding hadrons, and the multichain fragmentation model [31].

The paper is organized as follows. In Sec. II we discuss the basic string equations of motion and give some examples. In Sec. III the decay mechanism and its application to e^+e^- collisions is studied. Section IV discusses the details of the quark structure function fits via an ensemble of strings with different end-point dynamics. Section V introduces the interaction mechanisms between strings, and the model is used to study p-p high-energy collisions. We conclude the paper with a discussion of the model parameters and future applications.

II. RELATIVISTIC STRINGS

A. String equations

In this section we outline the basic properties and equations for relativistic, open classical strings. Some of the historical developments concerning the relativistic strings have already been mentioned in the Introduction [10]. The ultimate success of general string theories will not be known for some time. However, classical strings serve as a phenomenological tool to study the physics of extended confined objects [32]. The derivation of the string equations of motion is considerably involved. Here, we will only give an outline of the basic equations and concentrate on the physical picture of the string motion. More detailed derivation of the equations can be found in Refs. [33, 34]. We work in natural units where $\hbar = c = 1$.

The action of the relativistic strings is constructed in analogy with the action of a free particle. While the free-particle action is proportional to the length of its world line, the string action is proportional to the invariant area swept by the string. The string is defined to be a finite curve in space which sweeps out a hypersurface in four-dimensional space-time. The two-dimensional surface can be parameterized in terms of the general coordinates τ and s as $x^\mu(\tau, s)$. Figure 1 shows an illustration of this string motion. For a two-dimensional surface embedded in four-dimensional space-time the area element is [33]

$$dA = \left[\left(\frac{\partial x^\mu}{\partial s}\frac{\partial x_\mu}{\partial \tau}\right)^2 - \left(\frac{\partial x^\mu}{\partial s}\frac{\partial x_\mu}{\partial s}\right)\left(\frac{\partial x^\nu}{\partial \tau}\frac{\partial x_\nu}{\partial \tau}\right)\right]^{\frac{1}{2}} ds d\tau$$

which is used to define the string action as

$$\mathcal{S} = -\kappa \int dA = \int_{\tau_i}^{\tau_f} d\tau \int_0^S ds\, \mathcal{L} ,$$

$$\mathcal{L} = -\kappa \left[\left(\frac{\partial x^\mu}{\partial s}\frac{\partial x_\mu}{\partial \tau}\right)^2 - \left(\frac{\partial x^\mu}{\partial s}\frac{\partial x_\mu}{\partial s}\right)\left(\frac{\partial x^\nu}{\partial \tau}\frac{\partial x_\nu}{\partial \tau}\right)\right]^{\frac{1}{2}} ,$$

where κ is the string tension. The time over which the action is to be considered is defined by an initial time τ_i and a final time τ_f. The string ends are defined to be $s = 0$ and $s = S$, and κs represents the accumulative energy of the string from its zero end point to any other point along the string. Thus, the total energy of the string is κS. The initial and final configurations of the string will be those seen by a definite observer at a given instant of time in his Lorentz frame. This action is invariant under general string coordinate transformations and satisfies energy-momentum conservation.

General equations of motion and the boundary conditions are obtained by small variations of the surface that joins the initial and final configurations of the string. Due to the arbitrariness of the parametrization of the surface swept by the string we can choose additional coordinate conditions (Virasoro gauge conditions) which simplify the equations of motion. We work with the *orthonormal* parametrization

$$\frac{\partial x^\mu}{\partial s}\frac{\partial x_\mu}{\partial \tau} = 0 , \tag{1}$$

which implies that the velocity of a point along the string is always perpendicular to the string. We also note that the motion perpendicular to the string is timelike whereas motion along the string is spacelike. With this choice, the equations of motion reduce to the wave equation

$$\frac{\partial^2 x^\mu}{\partial \tau^2} - \frac{\partial^2 x^\mu}{\partial s^2} = 0 , \tag{2}$$

with the additional coordinate conditions

$$\left(\frac{\partial x^\mu}{\partial \tau}\right)^2 + \left(\frac{\partial x^\mu}{\partial s}\right)^2 = 0 , \tag{3}$$

and Eq.(1). In the following we choose the coordinates such that [33] $x^0(\tau, s) = \tau = ct$ and $\mathbf{x} = \mathbf{x}(\tau, s)$. Therefore, at the end points of the string, Eq.(3) gives

$$\frac{\partial \mathbf{x}(\tau, s)}{\partial t} = 1 , \tag{4}$$

which means that the end points move at the speed of light. As we shall see below the end points may be interpreted as massless quarks attached to each other via the string. We also obtain the spatial end-point boundary conditions

$$\frac{\partial x^\mu(\tau, 0)}{\partial s} = \frac{\partial x^\mu(\tau, S)}{\partial s} = 0 , \tag{5}$$

which tell us that there is no energy-momentum transfer out from the string end points.

The solution of Eq.(2) subject to the above coordinate conditions and the first of the conditions in Eq.(5) give

$$x^\mu(\tau, s) = \frac{1}{2}\left[y^\mu(\tau + s) + y^\mu(\tau - s)\right] , \tag{6}$$

where we have defined $y^\mu(t) \equiv x^\mu(t, 0)$, which is the trajectory of a single end point. This indicates that the entire string can be constructed from the knowledge of the trajectory of a single end point. The application of the second boundary condition in Eq.(5) results in the end-point periodicity equation

$$y^\mu(\tau + S) = y^\mu(\tau - S) + \frac{2P^\mu}{\kappa} , \tag{7}$$

where P^μ is the total four-momentum of the string and is given by

$$P^\mu = \kappa \int_0^S ds \frac{\partial x^\mu}{\partial \tau} . \tag{8}$$

Equation (7) is a periodicity condition for the equations of motion. Thus, if at time $\tau = 0$ the trajectory values of $\mathbf{y}(s)$ are known from $s = -E/\kappa$ to $s = E/\kappa$, and the momentum $\mathbf{P}$ is also known, then one can compute $\mathbf{y}$ for all times. This general procedure is illustrated in Fig. 2. Here, the curve labeled $\mathbf{y}(\tau)$ describes the trajectory of one of the end points. To construct the entire string at time, say, $\tau = 0$, we draw the vectors from $\mathbf{y}(0)$ to an arbitrary distance $\pm s$ along the trajectory. The location of the string point $\mathbf{x}(0, s)$ is then given by Eq.(6). Similarly, the vector from $\mathbf{y}(-s)$ to $\mathbf{y}(s)$ is proportional to the momentum of this string point via the generalized version of Eq.(7). At this point we also note that

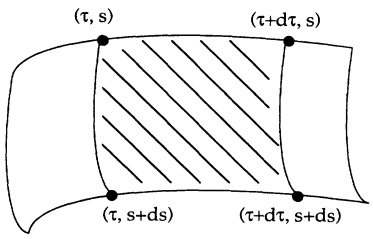

FIG. 1. The motion of a string in four-dimensional hypersurface. The invariant area dA is shown by the shaded area.

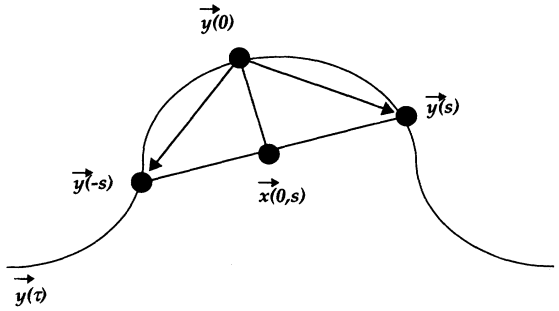

FIG. 2. The construction of a string from the trajectory of one of its end points. The details are explained in the text.

linear segments of the end-point trajectory will lead to multiple "hit" points. These points will have a larger energy-momentum content. Further details of the discrete numerical implementation of the string equations will be published elsewhere [34].

Finally, we will give expressions for the mass, energy, and momentum of the string and discuss the determination of the string tension κ. From Eq.(1) we can write

$$\left(\frac{\partial \mathbf{x}}{\partial s}\right)^2 = 1 - \mathbf{v}_\perp{}^2 = \frac{1}{\gamma^2} , \tag{9}$$

where we have defined $\mathbf{v}_\perp = \partial \mathbf{x}/\partial \tau$. In this notation an infinitesimal length element of the string $d\ell = |\partial \mathbf{x}/\partial s|\, ds = ds/\gamma$. We see that length is not a Lorentz-invariant quantity. The mass of an infinitesimal element of length $d\ell$ is

$$dm = \kappa d\ell , \tag{10}$$

which leads to expressions for the energy and momentum of the segment [see Eq.(8)]

$$\begin{aligned} dE &= \gamma dm = \kappa \gamma d\ell = \kappa ds , \\ d\mathbf{p} &= \kappa ds \mathbf{v}_\perp = \kappa \gamma \mathbf{v}_\perp d\ell . \end{aligned} \tag{11}$$

The string tension along the string is given by

$$\begin{aligned} \mathbf{T} &= \kappa \frac{\partial \mathbf{x}}{\partial s} , \\ |\mathbf{T}| &= \frac{\kappa}{\gamma} = \kappa \left(1 - \mathbf{v}_\perp{}^2\right)^{1/2} . \end{aligned} \tag{12}$$

For string pieces at rest ($\gamma = 1$) this gives $|\mathbf{T}_0| = \kappa$. To determine the approximate value of κ from Regge slopes, we calculate the mass and angular momentum of a string which, in its rest frame, is a rod of length $2a$ and its end points are rotating at the speed of light. The motion of the string traces a circle of radius a and the $v_\perp$ of a point at a distance r along the string is $v_\perp = r/a$. The expression for the total mass and angular momentum of the string is obtained from Eqs.(11)

$$\begin{aligned} M &= 2\int_0^a \frac{\kappa dr}{\sqrt{1 - v_\perp^2}} = \kappa a \pi , \\ J &= 2\int_0^a \frac{\kappa r dr v_\perp}{\sqrt{1 - v_\perp^2}} = \frac{\kappa a^2 \pi}{2} . \end{aligned} \tag{13}$$

We see from above that $J \propto M^2$ which is the desired Regge slope behavior. The slope $1/(2\pi\kappa)$ is equated to the experimental slope of 0.9 GeV^{-2} giving $\kappa = 0.88$ GeV/fm [35]. This is the value of κ used in our calculations.

B. Examples

In this section we will illustrate some examples of strings having different end point dynamics that will be used in constructing ensembles of strings which approximately reproduce the quark structure functions. In general, we classify the different string shapes by the motion of one of its end points.

One-dimensional motion of the end points along a line is the simplest string motion, and is commonly referred to as yo-yo motion. At a particular time the end points will be either approaching or receding away from each other at the speed of light. At the maximum stretch, which is determined by the invariant mass of the string at rest, all of the energy is contained in the string. At other times a part of the total energy is contained in the end points. When the two end points overlap at the center, the entire energy is contained at that point. This is illustrated in Fig. 3(a), which shows the light-cone coordinates for the yo-yo. The motion of one end-point trajectory is given by the solid line, while the other is given by the dashed line. The end-point energies change as the yo-yo moves, as illustrated by the changing size of the circles at the ends of the string. Note that at maximum stretch the end points contain no energy-momentum. At the point where the trajectories cross the string reduces to a point, as shown by the shaded circle. Figure 3(b) demonstrates the change in the yo-yo motion after an arbitrary Lorentz boost in the longitudinal direction. The area swept by

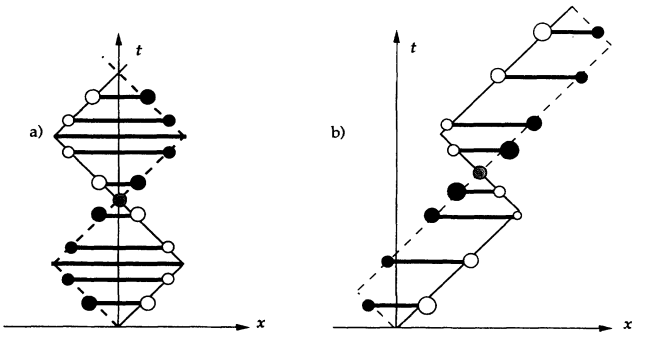

FIG. 3. (a) The motion of a string with end points executing one-dimensional (yo-yo) motion. The solid curve represents the motion of one of the end points and the dashed curve the other. The details are explained in the text. (b) A boosted one-dimensional string is illustrated.

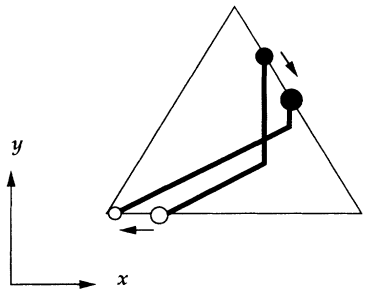

FIG. 4. The motion of a string with end points executing triangular motion is pictured. The details are explained in the text.

the yo-yo remains unchanged due to Lorentz invariance. The maximum length of a yo-yo with a mass of 0.94 GeV is 1.07 fm. A more complicated string structure corresponds to the triangle end-point trajectory. This is illustrated in Fig. 4 where the end point traces out an equilateral triangle in the x-y plane (time motion is projected onto the x-y plane). The string at two different times is pictured. In this case we note that a *kink* develops along the string. Kinks move at the speed of light along the string [32]. Note also the changing energy-momentum of the end points as the string moves, as illustrated by the changing size of the circles.

It is easy to imagine the extension of the above discussions to end-point trajectories of different types of triangles as shown in Fig. 5. The difference between various string structures manifests itself in the details of the string motion, and more importantly in the amount of the total string energy carried by the end points. In Sec. IV we utilize these properties to discuss the quark structure functions in the string picture.

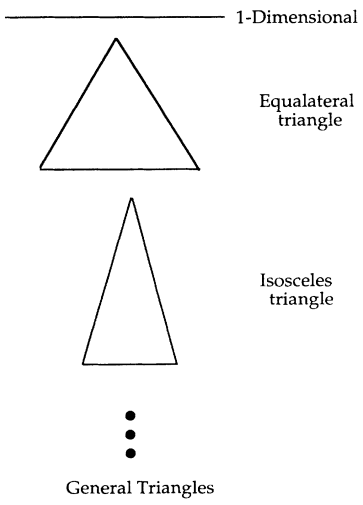

FIG. 5. Various shapes that illustrate the end-point motion of the strings.

III. HADRONIZATION MECHANISM

In order for the string picture to address the physics of strongly interacting high-energy particles, it must incorporate the hadronization process leading to color singlet final-state hadrons. The hadronization process is believed to take place via soft nonperturbative mechanisms which cannot be calculated by perturbation theory. Below, we will outline an adiabatic approach for string fragmentation. In addition, we will introduce a method for assigning transverse momenta to the created $q\bar{q}$ pairs. The formalism will be used to study the hadronization process in e^+e^- collisions.

A number of fragmentation models already exists. These models mainly fall into two categories. The independent jet models [36] assume that each parton fragments independently into colorless hadrons until all of the energy is exhausted. The choice of fractional momentum and other quantum numbers are assigned by a Monte Carlo scheme. The fragmentation functions are parameterized to reproduce the data. The independent jet models do not include color confinement even at a conceptual level, the energy and momentum are not conserved, and the results are not Lorentz invariant. These problems are cured by a reshuffling of energy, momentum, and other quantum numbers [19]. In contrast, the string fragmentation models [28] developed mainly by the LUND group are conceptually confined. In addition, it is generally believed that hadronization takes place via the decay of colorless objects [19]. Here, the color singlet string breaks into smaller strings as a consequence of quark-antiquark pair production along the string. This mechanism is also used for flux-tube breaking in strong-coupling QCD calculations [18]. The energy and momentum is conserved at each step of the fragmentation. As in the independent jet models it is possible to use fragmentation functions which are parameterized to reproduce the data and solve the fragmentation problem iteratively. However, an alternative approach was provided in Ref. [32] which assumed that the probability of creating a massless $q\bar{q}$ pair by a piece of a string of length $d\ell$ in time $d\tau$ is given by $Pd\ell d\tau$, where P is a constant. This approach does not require any iteration and the mass spectrum is directly obtained. Although this model gives a continuous mass spectrum, the approach can be modified to obtain a discrete mass spectrum [37, 38].

In essence our approach is similar to the string breaking models discussed above. The primary strings representing a nucleon have a quark on one end and a diquark on the other. However, the large part of the inclusive charged particle cross sections are mesons, corresponding to strings with end points having a quark and an antiquark. The mechanism of breaking the string via $q\bar{q}$ production can explain the meson multiplicities observed in experiments. In this approach one assumes that the stretching color flux tube breaks via the creation of a $q\bar{q}$ pair provided the color field of the new pair is equal and opposite to that of the parent string. This ensures that no qq strings are created. As the new q and $\bar{q}$ move away from each other, they absorb energy and

momentum from the parent string until the pair comes onto the mass shell. The actual mechanism that leads to the creation of $q\bar{q}$ pairs is not completely understood [40]. Various phenomenological models have been suggested [39,16]. These models are usually the extensions of the Schwinger mechanism for pair production in uniform external electromagnetic fields and in two-dimensional QED [41]. In the case of strings, the field creating the pairs is not external but arises from the color interactions between quarks. Although such models are intuitively appealing, a precise treatment of the particle production process requires a better understanding of the color field formation and color dynamics and is a difficult problem of quantum chromodynamics.

In our simulation of high-energy collisions, string-string interaction mechanisms lead to excited strings which stretch. A number of decisions must be made as to which strings are allowed to decay and once this condition is satisfied at which points the string should decay. The strings are usually allowed to decay until they reach a predefined minimum mass. In Fig. 6 we illustrate our approach. Here, point A represents the quark end and point D is the antiquark (or diquark) end. Point B is located such that the invariant mass of the string piece AB equals a cutoff mass M_{cq} [from Eq.(8) with $x^0 = \tau$]

$$M_{cq}^2 = \left(\kappa \int_A^B ds\right)^2 - \left(\kappa \int_A^B ds \frac{\partial \mathbf{x}}{\partial \tau}\right)^2 . \tag{14}$$

Similarly, we locate point C such that the invariant mass of the string piece DC equals the diquark mass cutoff M_{cqq}^2. The string is allowed to decay between the points B and C provided we can find points B and C satisfying the condition $A < B < C < D$.

The choice for the decay point is based on a probabilistic decay law obtained as follows: Assume that a small string segment has a probability of decay for an area swept out during the proper time interval, $d\tau$. The explicit expression for the area swept by the string segment is given by

$$\delta A_i = \left(1 - \mathbf{v}_{i\perp}{}^2\right) d\tau ds_i = \frac{d\tau (\Delta m_i)^2}{\kappa(\Delta \epsilon_i)} , \tag{15}$$

where the last equality follows from Eqs.(11). The probability that the piece will survive as the area increases by dA_i is given by ΛdA_i, where Λ is the decay rate, in units of fm^{-2}. In the limit of infinitesimal δA_i we thus obtain a simple rate equation:

$$\frac{dP(\delta A_i)}{dA_i} = -\Lambda P(\delta A_i) . \tag{16}$$

This equation is easily solved to give the following decay probability for an infinitesimal piece of string:

$$\bar{P}(\delta A_i) = 1 - P(\delta A_i) = 1 - e^{-\Lambda \delta A_i} \approx \Lambda \delta A_i . \tag{17}$$

The decaying piece is chosen by generating a random number with the above probability distribution. Note that this decay occurs locally, and ensures causality for the string breaking process. The probability for a piece of string to decay is the same in all Lorentz frames since it is a function only of a Lorentz invariant. This simple decay law, combined with the string dynamics, produces many of the gross features observed in high-energy fragmentation as follows: (*i*) The string breaking will commonly occur where the string stretches most, leading to the observed pionization, (*ii*) the pion distribution is somewhat uniform and produces a rapidity plateau, and (*iii*) since the primary quarks are at the ends of a string and fragmentation begins in the central region the string pieces containing the primary quarks fragment latest, thus producing the leading-particle effect.

The pair creation process is expected not only to reproduce the longitudinal distributions observed in high-energy collisions but also to contribute to the transverse momentum distributions. The quark and the antiquark of the created pair could carry equal and opposite non-vanishing transverse momenta. This source of transverse momenta will primarily contribute to the low-momentum (approximately $p_T \leq 1.0$ GeV) part of the total transverse momentum distribution. The high transverse momentum contributions may come from hard scatterings and processes such as the gluon bremmstrahlung. Although the transverse cross section comprises a small part of the total cross section, it is of significant importance in relativistic heavy-ion collisions since it could be used as a measure of the *stopping* experienced by the nuclei [42]. Various models of $q\bar{q}$ pair production [39] predict a Gaussian transverse momentum distribution which falls far short of the experimental distributions. Extensions of such models to infinitely long, uniform color-electric flux tubes with finite transverse size may be a remedy [43]. However, in the absence of any fundamental calculations we chose to parameterize the transverse momentum assignment with a simple exponential distribution function

$$f(p_T) p_T dp_T \propto e^{-\alpha p_T} p_T dp_T . \tag{18}$$

In making momentum assignments using Eq.(18) one must take into consideration the cutoff masses mentioned above. This is due to the fact that the energy-momentum of the created quarks must directly come from the string. To illustrate this process let us assume a decaying parent string with its invariant mass and velocity given by

$$M_p^2 = E^2 - \mathbf{P}^2, \boldsymbol{\beta}_p = \frac{\mathbf{P}}{E} . \tag{19}$$

The criteria for decay and the location of the decay point are chosen as described above. At the point of decay we assume that the $q\bar{q}$ pair is created with each member having equal but opposite transverse and longitudinal momenta. The longitudinal direction is defined as the rel-

FIG. 6. An illustration of the process for allowing a string to decay. The details are explained in the text.

ative momentum direction of the newly created strings in the rest frame of the parent string. The transverse direction is of course orthogonal to the longitudinal direction in this rest frame. At the time of creation quarks are virtual and each quark has a negative invariant mass squared

$$M_q^2 = -\left(p_T^2 + p_\ell^2\right) . \tag{20}$$

For each quark to come on mass shell, this mass must be compensated by the invariant mass of the string piece containing the quark. If initially the string piece has an invariant mass M_i^2, the total available invariant mass is $(M_i^2 - M_{cq}^2)$, which is due to the restriction that strings with mass smaller than the cutoff mass cannot be produced. This limits the maximum transverse momentum that could be assigned to the quark by the relation

$$\begin{aligned} &\left(M_i^2 - M_{cq}^2\right) + M_q^2 = 0 , \\ &p_T = \frac{1}{\sqrt{2}}\sqrt{M_i^2 - M_{cq}^2} , \end{aligned} \tag{21}$$

where we have made the ansatz that $|p_\ell| = |p_T|$ [39]. The direction of p_ℓ is chosen such that the quark obtains $M_q = 0$ in the shortest amount of time in the parent string rest frame. With these choices the momentum of the quarks produced in the rest frame of the decaying string will be directed in the transverse direction when the quark obtains $M_q = 0$. In practice, the decaying string is first boosted to its rest frame. After this, we calculate the maximum transverse momentum allowed for each of the quarks from Eq.(21). We also choose a random p_T value from the distribution of Eq.(18). The minimum of the three different momenta is chosen as the transverse and the longitudinal momentum of the virtual quarks. Subsequently, the string is boosted back to the velocity β_p frame. At this time the end points are still virtual and move longitudinally along the string at the speed of light. During this motion the quark absorbs the energy of the string until it arrives on the mass shell $(M_q^2 = 0)$. The proper time for this process can be viewed as the formation time for particle production. During the time when the quarks are virtual the strings are not allowed to interact or decay.

Parameters for decay were chosen as follows. The cutoff masses are chosen to obtain the experimental multiplicities in high-energy e^+e^- collisions. We have determined the cutoff mass M_{cq} to be = 0.25 GeV. The cutoff mass M_{cqq} is set equal to = 0.25 GeV for the e^+e^- calculations, whereas in hadron-hadron collisions it is equal to the proton mass. The decay rate is chosen to be 1.0 fm^{-2} which is commensurate with decay rates used in the LUND simulation programs. In principle, parameter Λ and the cutoff masses can be fine-tuned. This was not done for this work. Finally, we note that the average experimental transverse momentum is related to α in Eq.(18) by $< p_T >= 2/\alpha$. We have found that $\alpha = 3.88$ (GeV/c)$^{-1}$ produces the experimental low transverse momentum distributions fairly accurately with $< p_T > \approx 0.350$ GeV/c. This difference is due to the restrictions arising from the cutoff masses.

We have performed calculations for simulating e^+e^- collisions at a number of center-of-mass energies. The simulation starts from the point where the $q\bar{q}$ pair is created. This point is initialized as a yo-yo with both endpoints at the center position and the endpoints are assigned back-to-back velocities corresponding to the beam energy. The jet analysis is primarily performed along the jet axis which we have aligned with the z axis. Statistics were collected for $N_{\rm ev} = 1000$ collisions. The strings contained 2000 segments for the $\sqrt{s} = 14$ GeV simulations and 2300 segments for the $\sqrt{s} = 22$ GeV case. The time evolution was continued until the number of produced mesons reached a constant value. Since the experiments usually detect only charged particles, our total yields were adjusted for the neutrals by multiplying with a factor of 2/3. In Fig. 7 we plot the average charge particle multiplicity as a function of the center-of-mass energy. These results were used in fixing the quark and antiquark cutoff masses to be $M_{cq} = M_{cqq} = 0.25$ GeV. All of our data is from the TASSO experiments which are found in Refs. [44, 19]. All distributions are normalized to the number of events, $N_{\rm ev}$, where a single event is defined as one collision. In Fig. 8 we show the charge-particle distributions given by

$$\frac{dN}{dn_{\rm ch}}$$

which have been calculated at two different energies $\sqrt{s} = 14$, 22 GeV. Here, dN represents the number of charged particles in the interval $(n_{\rm ch}, n_{\rm ch} + dn_{\rm ch})$. We see that the results are in relatively good agreement with the experimental distributions except for very large particle numbers.

Another test of the decay scheme and the cutoff masses is the rapidity and the longitudinal momentum fraction distributions. Rapidity is defined as

$$y = \frac{1}{2}\ln\left(\frac{E + p_l}{E - p_l}\right)$$

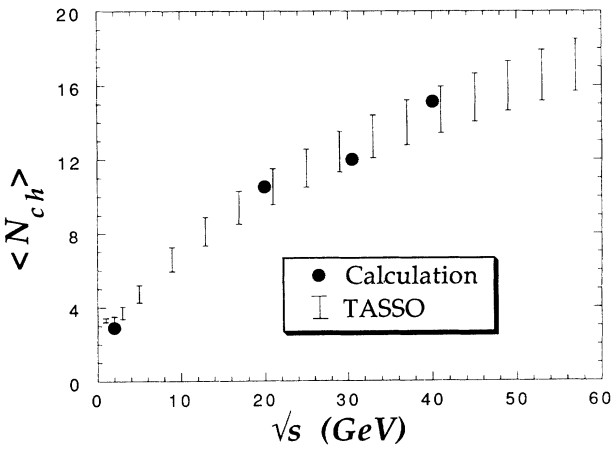

FIG. 7. e^+e^- average charged-particle multiplicities as a function of the center-of-mass energy. Lines show the experimental range and the solid circles are our calculations.

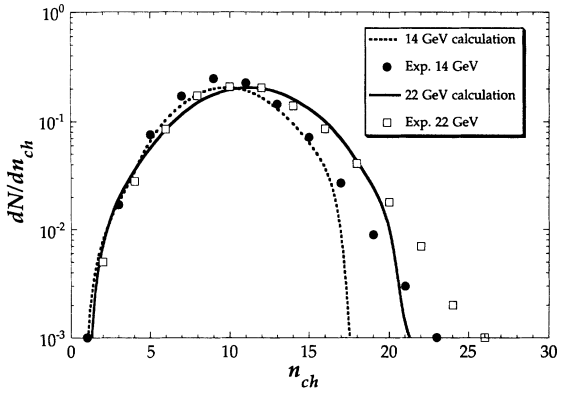

FIG. 8. e^+e^- multiplicity distributions. Data are from Ref. [44].

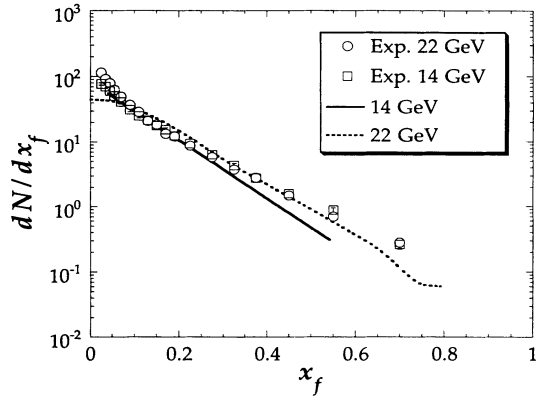

FIG. 10. e^+e^- charged-particle longitudinal momentum fraction distributions. Data are from Ref. [44].

where the longitudinal direction is along the jet axis. The longitudinal momentum fraction is given by $x_f = 2p_l/\sqrt{s}$. Results are shown for the rapidity in Fig. 9, and for x_f in Fig. 10. Although the comparison with the x_f distribution is fairly reasonable over a wide range of x_f values, the rapidity distribution is not well reproduced for large rapidity values. The choice of M_{cq}, which is determined from the total multiplicity, is a factor in the inability of the model to reproduce the tail in the high-rapidity region. High-rapidity particles are those that have masses near the pion mass which are excluded from our model due to the cutoff mass. Lowering the cutoff mass increases the large rapidity yields. Variation of the parameter Λ and the cutoff masses may improve the agreement with the data in the tail regions. Another alternative would be to use sets of different cutoff masses, some lighter than 0.25 GeV and some heavier. However, for the purposes of understanding the gross features of our model this is not necessary. Note also that the suppression of calculated events at low rapidity in comparison to data occurs since the inclusive data also includes heavy-quark production [45]. Finally, the transverse momentum distribution of the produced particles is shown in Fig. 11 for $\sqrt{s} = 14$ GeV and in Fig. 12 for $\sqrt{s} = 22$ GeV. The parameter α has not been adjusted for each energy. The results are in good agreement for $p_T < 1.0$ GeV/c whereas for larger p_T values the data is underestimated. The inclusion of the string-string interactions will be discussed in Sec. V. First we must consider the initial string states for the nucleons.

IV. STRUCTURE FUNCTIONS

In building the phenomenology of the dynamical string-parton-model description of relativistic heavy-ion collisions, it is desirable to start from a description which entails many of the features observed for more elementary high-energy processes. One of the most important properties of hadrons is their substructure, observed mainly via deep-inelastic charged lepton-hadron collisions [6,46]. The common feature of the high-energy data is the Q^2 (four-momentum transfer) independence of the structure functions for fixed values of the variable $x = Q^2/2M\nu$, where M denotes the nucleon mass and ν is the transferred energy. In the parton model this scaling behavior is explained in terms of the presence of pointlike charged

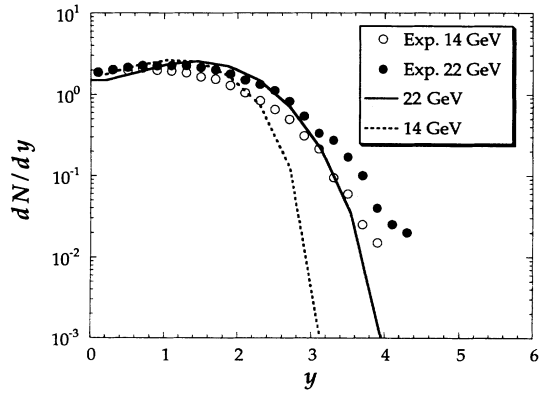

FIG. 9. e^+e^- charged-particle rapidity distribution. Data are from Ref. [44].

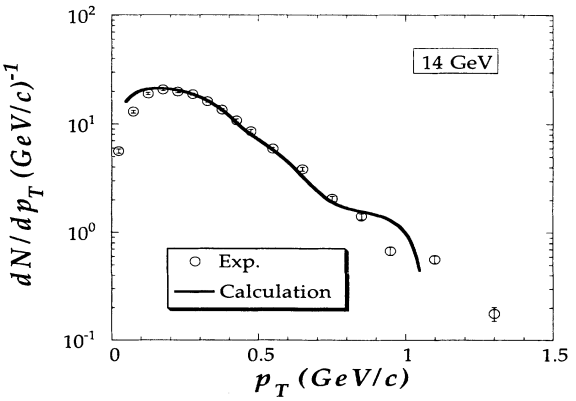

FIG. 11. e^+e^- calculated p_T distribution at $\sqrt{s} = 14$ GeV. Data are from Ref. [44].

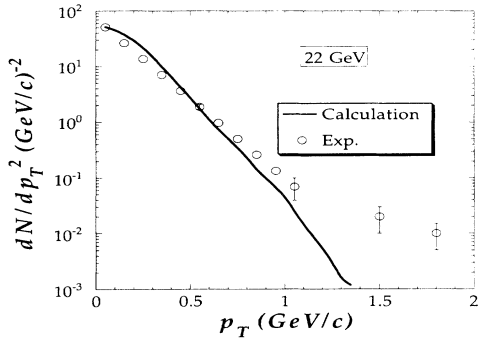

FIG. 12. Calculated p_T distribution at $\sqrt{s} = 22$ GeV. Data are from Ref. [44].

constituents generically called partons. The relationship between the two purely electromagnetic structure functions, F_1 and F_2 (in the scaling limit $F_2 = 2xF_1$), and the valence quark distributions of the nucleon can be obtained in the scaling limit by assuming that partons *are* quarks and that antiquarks, sea quarks, and quark flavors heavier than up and down quarks have the same flavor-independent distribution functions [8]. The quark distribution functions obtained from deep-inelastic e-p collisions [47] can be parametrized for convenience. Here, we use the Eichten, Hinchliffe, Lane, and Quigg (EHLQ) parametrization [48]

$$xu_v(x) = 1.78x^{0.5}\left(1 - x^{1.51}\right)^{3.5} ,$$
$$xd_v(x) = 0.67x^{0.4}\left(1 - x^{1.51}\right)^{4.5} , \tag{22}$$

where u_v and d_v are the valence quark distribution functions. The u_v distribution integrates to 2 and the d_v distribution to 1, giving

$$\frac{1}{3}\int_0^1 [u_v(x) + d_v(x)]\,dx = 1 , \tag{23}$$

and thus yielding a flavor-averaged *proton* distribution function

$$q_p = \frac{1}{3}\left[u_v(x) + d_v(x)\right] . \tag{24}$$

It can be shown in the infinite momentum frame that the scaling variable x is the fraction of the momentum of the nucleon carried by the struck parton. This relation is true only in this frame; however, it is approximately valid in other frames, if the partons are assumed to be massless. Corrections arising from the finite parton mass are usually neglected as well as the small differences between neutron and proton distribution functions [49].

In the relativistic string picture the string end points are interpreted as massless quarks moving at the speed of light. For the description of baryons one end represents a single quark whereas the other end represents a diquark. Each quark carries a baryon number of 1/3 thus giving $B = 1$ for baryons. The description of mesons involves a quark at one end, and an antiquark at the other. In addition, as we have discussed in a previous section for a yo-yo and a triangle string, the end points contain a varying amount of the total string energy. In the case of the yo-yo in its rest frame, two end points carry the same amount of energy, which for a yo-yo of rest mass M and instantaneous length L is

$$E_q = \frac{M - \kappa L}{2} . \tag{25}$$

Thus, for relativistic strings, it is natural to define a fractional momentum variable associated with the string end points. Assuming collinear motion along the z direction, which will be the boost axis, we define the string longitudinal momentum fraction in terms of the ratio of the light-cone variables,

$$x_s = \frac{k_0 + k_3}{P_0 + P_3} , \tag{26}$$

where k is the end-point four-momentum and P is the total string four-momentum. The variable x_s is Lorentz invariant for boosts in the longitudinal direction. In the rest frame of a yo-yo string, the maximum x_s that can be attained by an end-point is

$$(x_s)_{\max} = \frac{k_0 + k_3}{P_0} = \frac{\frac{1}{2}P_0 + \frac{1}{2}P_0}{P_0} = 1 , \tag{27}$$

whereas for a triangle trajectory the same quantity becomes

$$(x_s)_{\max} = \frac{\frac{1}{3}P_0 + \frac{1}{3}P_0}{P_0} = \frac{2}{3} . \tag{28}$$

This can be generalized to arbitrary triangles where the maximum length of one side is a fraction a of the total perimeter of the triangle. We then have

$$(x_s)_{\max} = \frac{aP_0 + aP_0}{P_0} = 2a . \tag{29}$$

In order to construct a distribution function we consider the probability for finding a string end point with a momentum fraction x_s. As we have seen in a previous section the string end points move in time and change their energy-momentum content. Furthermore, Eq.(26) also indicates a dependence on the orientation of the end-point trajectory with respect to the boost axis. Thus, the probability depends on two independent variables, time t and the orientation angle θ, and can be described by the function $\mathcal{P}_i(x_s;t,\theta)$, where the index i identifies strings with different end-point dynamics. θ is defined as the angle between the normal to the plane in which the end-point trajectory lies and the boost axis in the rest frame of the string. Averaging this distribution over one time period and over all possible orientations defines the distribution function for a particular string:

$$q_i(x_s) = \frac{1}{2T}\int_0^T dt \int_0^\pi \sin\theta d\theta \mathcal{P}_i(x_s;t,\theta) . \tag{30}$$

The functions $q_i(x_s)$ approach frame independence for large γ, in accordance with the parton model. Actually $\gamma \geq 5$ yields nearly frame-independent distribution functions. Since strings with different end-point dynamics

TABLE I. Relative weights of various string types used in reproducing the proton structure function in the string-parton model.

End-point dynamics	Weight
C_1	0.0907
C_2	0.4402
C_3	0.2261
C_4	0.2430

correspond to different values for $(x_s)_{\max}$, an ensemble of such strings can be used to reproduce the proton structure function $q_p(x)$ of Eq.(24). We denote this ensemble by

$$q_{sp}(x_s) = \sum_i \rho_{i/p} = \sum_i C_i q_i(x_s) , \tag{31}$$

where q_{sp} is the calculated valence quark distribution function for the proton p, and C_i denotes the weight of the type i string in our ensemble. We choose, for our ensemble end-point dynamics of the yo-yo ($i = 1$), isosceles triangles with sides whose lengths are in the ratio 0.4 : 0.4 : 0.2 ($i = 2$) and 0.45 : 0.45 : 0.1 ($i = 3$), and equilateral triangles ($i = 4$). Since the ranges of x_s values for strings executing different end-point motion do not fully overlap, the coefficients C_i can be determined by first requiring the equivalence of $q_p(x_s)$ and $q_{sp}(x_s)$ at various values of x_s. Since only the yo-yo trajectory x_s is nonzero in the region $0.9 < x_s < 1.0$, we choose

$$C_1 = \frac{q_p(x_s = 0.9)}{q_1(x_s = 0.9)} , \tag{32}$$

where we have chosen the point $x_s = 0.9$ in demanding the equality. Similarly, C_2 is obtained by first subtracting the yo-yo contribution from $q_p(x_s)$ and requiring that for $x_s = 0.8$ the $i = 2$ trajectory reproduces the structure function

$$C_2 = \frac{q_p(x_s = 0.8) - C_1 q_1(x_s = 0.8)}{q_2(x_s = 0.8)} . \tag{33}$$

C_3 is found in a similar fashion at $x_s = 2/3$, and

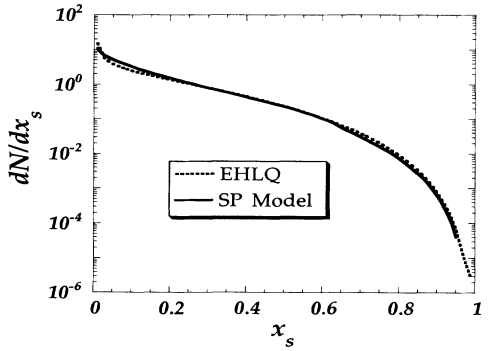

FIG. 13. A fit to the flavor-averaged proton distribution function using an ensemble of strings with different end-point dynamics. The solid curve denotes our calculations and the EHLQ parametrization is given by the dashed line.

$C_4 = 1 - C_3 - C_2 - C_1$. Table I gives the coefficients found for this selection. The corresponding agreement between $q_p(x_s)$ and $q_{sp}(x_s)$ is shown in Fig. 13. As we see the agreement is generally very reasonable. This ensemble will be used when performing string-parton model calculations of collisions involving protons.

V. HADRON-HADRON COLLISIONS

A. Interactions

For the simulation of relativistic hadron-hadron collisions an interaction mechanism between two evolving strings must be introduced. Historically, the suggested mechanism had been the exchange of arms between two overlapping strings [32]. The application of this approach to dynamical strings [20] provided only a small fraction of the total p-p cross section and had to be supplemented by the assumption of a "flux-tube radius" for the strings [43]. This nonlocal interaction mechanism has been justified as being due to the vacuum fluctuations of the gluon field. On the other hand, the modified arm exchange mechanism does not make any contact with the relatively well known limits of the strong interaction dynamics. The quarks are merely spectators in all interactions having only the task of creating large uniform chromoelectric flux tubes. This is in contrast with the understanding of hadron-hadron collisions in terms of the parton model and QCD model calculations. In the large-Q^2 limit (where Q denotes the four-momentum transfer), there is considerable evidence that constituent quarks behave as pointlike particles and undergo hard scatterings [6–8]. Such hard scatterings are believed to be the main source of high-p_T production in hadron-hadron collisions [22]. Similarly, in the low-Q^2 regime the hadrons can interact via quark or other exchange mechanisms and still preserve their color-singlet nature. Such mechanisms have been applied to construct potential models for the hadron-hadron interactions [25]. Experimental studies of jets in hadron-hadron and e^+e^- collisions also indicate that the hadronization mechanism occurs from color-neutral objects [19] suggesting that the color-singlet nature of the strings must be preserved during the interaction. In this section we incorporate these features into the string model via the introduction of phenomenological interactions between the string end points.

In previous work that involved parton-parton collisions, a classical radius of interaction was chosen [50]. In the following we present a brief outline of parton-parton scattering theory which has been used in this work. We consider the scattering of two nucleons for which the interaction takes place between constituent partons. Factorization [51] may be used to write the nucleon-nucleon cross section in terms of the parton-parton cross sections. The nucleon-nucleon cross section is then

$$\omega_{AB} d\sigma = \sum_{ij} dx_A dx_B \rho_{i/A}(x_A) \rho_{j/B}(x_B) \omega_{ij} d\sigma_{ij} ,$$

where

$$d\sigma_{ij} = \sum_{\alpha\beta} |\langle f'_\alpha f'_\beta | S | f_i f_j \rangle|^2 d^2b . \tag{34}$$

The expression $\rho_{i/A}(x_A)dx_A$ gives the probability of finding a parton of type i in nucleon A with momentum fraction between x_A and $x_A + dx_A$. The normalization is given by $\omega_{AB} = 2\omega_A 2\omega_B$ and $\omega_{ij} = 2\omega_i 2\omega_j$. The cross section $d\sigma_{ij}$ denotes an inclusive observable summed over all final states, $|f'_\alpha f'_\beta\rangle$. In principle we could evaluate the scattering into definite final states (f'_a, f'_b); however, in our treatment it is advantageous to use completeness of these states and replace them by a complete set of free-particle states such that

$$\begin{aligned} d\sigma_{ij} &= \sum_{\alpha\beta} \langle f_i f_j | S^\dagger | f'_\alpha f'_\beta \rangle \langle f'_\alpha f'_\beta | S | f_i f_j \rangle d^2b \\ &= \sum_{p'_1 p'_2} \langle f_i f_j | S^\dagger | p'_1 p'_2 \rangle \langle p'_1 p'_2 | S | f_i f_j \rangle d^2b \\ &= \sum_{p'_1 p'_2} |\langle p'_1 p'_2 | S | f_i f_j \rangle|^2 . \end{aligned} \tag{35}$$

In order to calculate the cross sections, we must evaluate the scattering matrix, which is carried out in Ref. [52]. We briefly outline the strategy for this calculation here. We note that the initial state may be expanded in terms of impact-parameter-dependent wave packets:

$$|f_i f_j\rangle = \int d\tilde{p}_i d\tilde{p}_j f_i(p_i, \mathbf{b}) f_j(p_j, \mathbf{b}) |p_i p_j\rangle , \tag{36}$$

where $f_i(p_i, \mathbf{b})$ are peaked about $\bar{p}_i$, and

$$d\tilde{p} = \frac{d^3p}{(2\pi)^3 2\omega_p} .$$

The impact-parameter dependence of f is given by

$$f_i(p_i, \mathbf{b}) = g_i(p_i) \exp(-i\mathbf{p}_{i\perp} \cdot \mathbf{b}/2) , \tag{37}$$

$$f_j(p_j, \mathbf{b}) = g_j(p_j) \exp(i\mathbf{p}_{j\perp} \cdot \mathbf{b}/2) . \tag{38}$$

Following the standard derivation [53], we define the invariant scattering matrix element as

$$\begin{aligned} \langle p'_1 p'_2 | S | p_1 p_2 \rangle = {} & \mathcal{M}(p_1 p_2; p'_1 p'_2) \\ & \times (2\pi)^4 \delta^4(p_1 + p_2 - p'_1 - p'_2) . \end{aligned}$$

Using the assumption of highly peaked wave packets, we obtain the expression for the impact-parameter-dependent scattering matrix:

$$\begin{aligned} |\langle p'_1 p'_2 | S | f_i f_j \rangle|^2 = {} & \mathcal{F}_{ij}(\mathbf{b}) |\mathcal{M}(\bar{p}_i \bar{p}_j; p'_1 p'_2)|^2 \\ & \times (2\pi)^4 \delta^4(\bar{p}_i + \bar{p}_j - p'_1 - p'_2) , \end{aligned}$$

where the impact-parameter-dependent function $\mathcal{F}(\mathbf{b})$ is defined as

$$\mathcal{F}_{ij}(\mathbf{b}) = \int d^4x |f_i(x, \mathbf{b})|^2 |f_j(x, \mathbf{b})|^2 . \tag{39}$$

We assume that f_i and f_j are highly Lorentz contracted. Thus the longitudinal and transverse coordinate space dependence decouples, giving

$$|\tilde{f}_{i,j}(x, \mathbf{b})|^2 = \delta(z \pm \beta_{i,j} t) |f^{(\perp)}_{i,j}(\mathbf{x}_\perp \pm \mathbf{b}/2)|^2 , \tag{40}$$

where $\tilde{f}(x, \mathbf{b})$ is the Fourier transform of $f(p, \mathbf{b})$. Using this assumption for the parton wave packet, we find that

$$\begin{aligned} \mathcal{F}_{ij}(\mathbf{b}) &= \frac{1}{|\beta_i - \beta_j|} F_{ij}(\mathbf{b}) \\ &= \frac{1}{|\beta_i - \beta_j|} \\ &\quad \times \int d^2x_\perp |f^{(\perp)}_i(\mathbf{x}_\perp + \mathbf{b}/2)|^2 |f^{(\perp)}_j(\mathbf{x}_\perp - \mathbf{b}/2)|^2 . \end{aligned}$$

The function $F_{ij}(\mathbf{b})$ describes the overlap of the parton wave functions in terms of the impact parameter $\mathbf{b}$. Therefore, the impact-parameter-dependent cross section is given by

$$\begin{aligned} d\sigma_{ij} = \sum_{p'_1 p'_2} & \frac{1}{|\beta_i - \beta_j|} F_{ij}(\mathbf{b}) (2\pi)^4 \delta^4(\bar{p}_i + \bar{p}_j - p'_1 - p'_2) \\ & \times |\mathcal{M}(\bar{p}_i \bar{p}_j; p'_1 p'_2)|^2 d^2b . \end{aligned}$$

Note that

$$\int d^2b F_{ij}(\mathbf{b}) = 1 , \tag{41}$$

so that the impact-parameter-independent expression for the parton cross section is given by [53]

$$\begin{aligned} d\sigma_{ij} = \sum_{p'_i p'_j} & \frac{1}{|\beta_i - \beta_j|} \\ & \times (2\pi)^4 \delta^4(\bar{p}_i + \bar{p}_j - p'_1 - p'_2) |\mathcal{M}(\bar{p}_i \bar{p}_j; p'_1 p'_2)|^2 . \end{aligned}$$

The final expression for the impact-parameter-dependent cross section for nucleon-nucleon scattering is given by

$$\omega_{AB} d\sigma = \sum_{ij} dx_A dx_B \rho_{i/A}(x_A) \rho_{j/B}(x_B) \omega_{ij} \sum_{p'_1 p'_2} \frac{1}{|\beta_i - \beta_j|} F_{ij}(\mathbf{b}) (2\pi)^4 \delta^4(\bar{p}_i + \bar{p}_j - p'_1 - p'_2) |\mathcal{M}(\bar{p}_i, \bar{p}_j; p'_1, p'_2)|^2 d^2b .$$

The invariant matrix element $\mathcal{M}$ may be calculated in terms of the Mandelstam variables for the quarks s, t, u, which are defined as

$$s = (\bar{p}_i + \bar{p}_j)^2 , \quad t = (\bar{p}_i - p'_2)^2 , \quad u = (\bar{p}_i - p'_1)^2 .$$

In the string model, since all interactions at this stage are mediated by the quarks, we use a phenomenological scattering, which includes the first Born order terms, for the quark scattering. The invariant matrix element is then given by

$$|\mathcal{M}(\bar{p}_i \bar{p}_j; p'_1 p'_2)|^2 = \alpha_t^* \frac{s^2 + u^2}{(t - m_t^2)^2} + \alpha_u^* \frac{s^2 + t^2}{(u - m_s^2)^2} ,$$

where α_t^*, α_u^* are strength parameters for the two scattering channels, and m_t, m_u are effective range parameters.

At this time $\alpha_t^* = \alpha_u^* = 0.7$ and $m_t = m_u = 1/r_\perp$, where $r_\perp$ is an effective range of the interaction between two quarks. In future work, as we move the model up in collision energy, we will be able to use these parameters to obtain the correct jet cross sections in proton-proton collisions. The present model does not include gg scattering processes and therefore it may be limited to intermediate energies where such processes are believed to be unimportant.

B. Implementation in the string-parton model

For numerical convenience we use a coordinate space theta function in terms of the quark impact parameter. Thus, when two partons are within an interaction distance $|\mathbf{b}| < r_\perp$ then the two partons will scatter with probability one. The quark wave functions are treated as theta functions in the current work. In a future paper we will perform this calculation with a more realistic choice for the parton wave functions [52]. The wave packet in the longitudinal direction for the partons has been infinitely contracted since the partons move at the speed of light. Therefore, in the present work, if two partons are within one time step of each other in the longitudinal direction they may interact. For a cross section of 30 mb, which is the inelastic cross section for proton-proton collisions, the effective range $r_\perp$ was found to be approximately 0.8 fm. This number is also commensurate with the model-dependent and -independent QCD estimates of the effective extent of the quarks inside hadrons [54]. The hadron-hadron calculations presented in this paper were done with approximately 1000 collisions. The general procedures for performing each hadron-hadron collision simulation using the string-parton model can be outlined as follows: Two strings are set up on the left and right of the reaction plane. The center point of the right string is placed at a point $(\rho/2, z_0)$ whereas the center point of the left string is at $(-\rho/2, -z_0)$, to simulate a collision with a string impact parameter ρ. Since the strings experience a large Lorentz contraction in the longitudinal direction when they are boosted, a safe choice for z_0 is 0.5 fm. Each string is randomly oriented in solid angle $d\Omega$ about its center. The type of the strings are randomly generated according to the expansion coefficients, C_α. This choice ensures that the simulation of left and right hadrons begins with the correct parton distribution functions. The strings are then boosted to a center-of-momentum frame such that the desired $\sqrt{s}$ is obtained. The strings propagate in time according to the string equations of motion. The overlap of the parton wave functions is then checked at each time step. The overlap determines a probability for the parton interaction, as discussed previously. This is carried out in the center-of-momentum frame of the quarks. Whether an end point is a quark or diquark is not assigned until after the collision, at which point it is assumed that the two end points that collide are quarks. There are four possible collision combinations. If more than one of the combinations is found to be interacting at any one time step, then the two quarks that are closest to each other in the quark center-of-momentum frame are selected. Two quarks which have scattered are rearranged on the strings in order to preserve the color singlet nature of the hadrons. Once they have interacted, strings are allowed to decay as discussed in Sec. III.

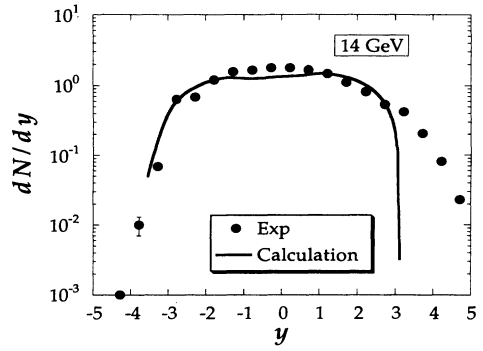

FIG. 14. Rapidity distributions of charged particles for pp collisions at $\sqrt{s} = 19.4$ GeV. Data are from Ref. [57].

C. Proton-proton collisions

We have performed simulations for p-p collisions at two different center-of-mass energies, $\sqrt{s} = 19.44$ and 53 GeV. For these energies strings were discretized using 1300 and 1990 points, respectively. Various distributions were obtained including the rapidity, x_f, and transverse momentum. The value of the quark cutoff mass was increased to $M_{cq} = 0.36$ GeV in order to obtain the correct total multiplicity of final particles. The diquark cutoff mass was set equal to the proton mass, $M_{cqq} = 0.94$ GeV. This readjustment is expected since the charged particle multiplicities in p-p collisions are approximately 20% lower than the e^+e^- collisions at the same center-of-mass energy [56]. In Fig. 14 we plot the calculated rapidity distribution of the final particles in comparison to the experimental results [57] at $\sqrt{s} = 19.4$ GeV. Similar to the e^+e^- case the agreement in the central rapidity region is good whereas the large-rapidity tails are not reproduced due to the large

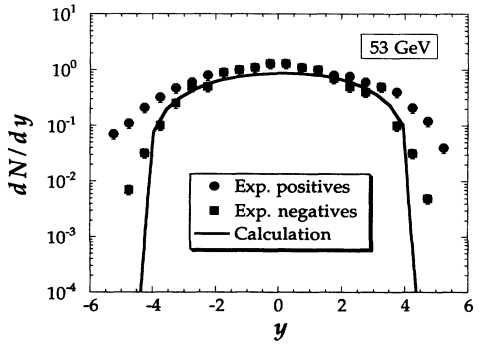

FIG. 15. Rapidity distributions of charged particles of positive and negative particles for pp collisions $\sqrt{s} = 53$ GeV. Data are from Ref. [58].

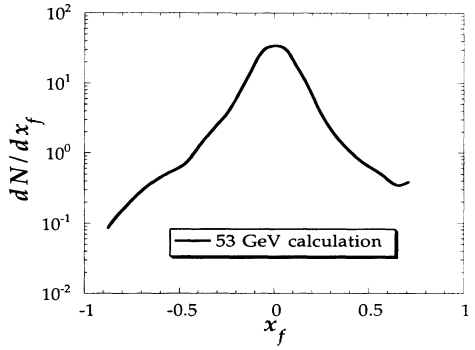

FIG. 16. The longitudinal momentum fraction variable x_f is shown for pp collisions at $\sqrt{s} = 53$ GeV.

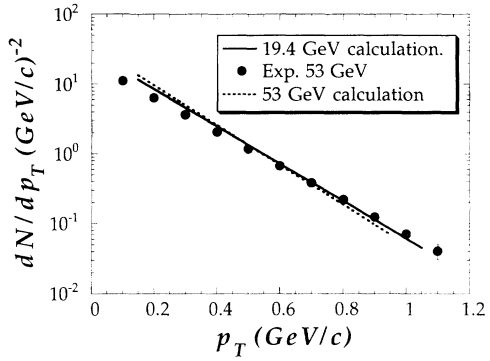

FIG. 17. The calculated transverse momentum distributions are shown for pp collisions at $\sqrt{s} = 19.4$ and $\sqrt{s} = 53$ GeV. Data for the two energies in this momentum range are similar, and only the 53-GeV data are plotted [58].

value of the cutoff mass, which inhibits the production of low-mass large-rapidity particles. In Fig. 15 we plot the rapidity distribution for $\sqrt{s} = 53$ GeV. The data show the experimental positive and negative charged-particle distributions [58] in comparison to our calculations. Finally, Fig. 16 shows the longitudinal momentum fraction distribution for $\sqrt{s} = 53$ GeV. The distributions show the familiar peak at $x_f = 0$. Figure 17 shows the calculated transverse momentum distribution at $\sqrt{s} = 19.4$ GeV and at $\sqrt{s} = 53$ GeV in comparison with the experimental results [58] at 53 GeV. The results are in good agreement up to the transverse momentum range considered in these calculations ($p_T < 1.1$ GeV/c). The scattering model discussed in the previous section would allow comparisons at much higher values for transverse momentum, however, the required statistical accuracy for the reproduction of the exponentially decaying distribution would require 50 000–100 000 collisions. These calculations will be performed in the future.

VI. CONCLUSION

We have presented a model based on the relativistic Nambu-Gotō string formalism for studying inclusive hadronic processes in high-energy collisions. The calculations are performed in four-dimensional space-time with no restrictions. We have shown that an ensemble of different string structures can be used to approximately reproduce the experimentally observed valence quark structure functions. This was achieved by the interpretation of string end points as quarks or diquarks. The interaction mechanism employs a $u-$ and $t-$ channel parton exchange interaction with phenomenological ranges and strengths. Excited strings decay according to an adiabatic decay scheme and the decay is interpreted as being due to $q\bar{q}$ production along the string. The produced quarks are assigned transverse momenta based on a phenomenological distribution. In this form the formalism successfully reproduces the gross features of the data from relativistic e^+e^-, e-p, and p-p collisions. These include the rapidity distributions, transverse momentum distributions, longitudinal momentum fraction distributions, and total charged-particle multiplicities. Due to the time-dependent nature of the model we also obtain meson and baryon formation times and the time development of various particle and energy densities. In Table II we tabulate the set of parameters used in the model and the criteria for their choice.

The string phenomenology has been a successful tool for performing simulations of strong interaction physics. Confinement is conceptually incorporated into the model, and other connections with QCD model calculations, as mentioned in the Introduction, make the string formalism an attractive approach for studying strongly interacting extended objects. An important caveat to stress at this point is that the connection of the model to the true nature of the strong-interaction dynamics is rather tenuous. This is particularly true for the formulation of quark-quark interactions and the $q\bar{q}$ production which are among the unresolved problems of quantum chromo-

TABLE II. Parameters of the model.

Symbol	Name	Method of determination	Value
κ	String tension	Regge slope	0.88 GeV/fm
$M_{cq}(e^+e^-)$	Meson mass cutoff	Total multiplicity	0.25 GeV
$M_{cq}(p-p)$	Meson mass cutoff	Total multiplicity	0.36 GeV
M_{cqq}	Baryon mass cutoff	Proton mass	0.94 GeV
Λ	Decay rate	LUND	1.0 fm^{-2}
$f(p_T)$, α	p_T distribution	Fit to e^+e^- data	3.88 (GeV/c)$^{-1}$
$r_\perp$	Interaction range	$p-p$ cross section	0.8 fm
α_s^*	Effective coupling constant	$p-p$ cross section	0.71

dynamics. Our goal is to develop an effective dynamical formalism which could be used for studying the hadronic interactions taking place during the collisions of relativistic heavy ions. The hope is that a better understanding of the hadronic debris would improve our chances of isolating the signals coming from the decay of the quark-gluon plasma. As it stands, the model is readily extendable to the studies of e-A, p-A, and A-A collisions. These computed intensive calculations are currently underway.

ACKNOWLEDGMENTS

This research was sponsored in part by the U.S. Department of Energy under Contract No. DE-AC05-84OR21400 with Martin Marietta Energy Systems, Inc. and under Contract No. DE-FG05-87ER40376 with Vanderbilt University. The numerical calculations were carried out on CRAY-2 supercomputers at the National Center for Supercomputing Applications, Illinois, at the National Energy Research Supercomputer Center, Livermore, and on the Intel iPSC/860 hypercube at the Oak Ridge National Laboratory. The authors also wish to acknowledge the Institute for Nuclear Theory at the University of Washington, Program III: Hard QCD Probes of Dense Nuclear and Hadronic Matter, 1990, where some of the development of the present work took place.

[1] *Quark Matter '88*, Proceedings of the Seventh International Conference, Lenox, Massachusetts, 1988, edited by G. A. Baym, P. Braun-Munzinger, and S. Nagamiya [Nucl. Phys. **A498**, 1 (1989)], and references therein; J. D. Bjorken, Phys. Rev. D **27**, 140 (1983).

[2] M. Bander, Phys. Rep. **75**, 206 (1981); J. Kogut, Rev. Mod. Phys. **55**, 775 (1983); M. Creutz, *Quarks, Gluons and Lattices* (Cambridge University Press, Cambridge, England, 1983); A. Hasenfratz and P. Hasenfratz, Annu. Rev. Nucl. Part. Sci. **35**, 601 (1985).

[3] A. Ukawa, Nucl. Phys. **A498**, 227c (1989); M. Fukugita, S. Ohta, Y. Oyanagi, and A. Ukawa, *Field Theory on the Lattice*, Proceedings of the International Symposium, Seillac, France, 1987, edited by H. Billoire [Nucl. Phys. B Proc. Suppl. **4**, 105 (1988)]; Phys. Rev. Lett. **58**, 2515 (1987); J. B. Kogut, J. Polonyi, H. W. Wyld, and D. K. Sinclair, Phys. Rev. D **31**, 3304 (1985).

[4] S. Gottlieb, W. Liu, D. Toussaint, R. L. Renken, and R. L. Sugar, Phys. Rev. Lett. **59**, 1513 (1987); **59**, 1881 (1987); **59**, 2247 (1987); Phys. Rev. D **38**, 2888 (1988); C. DeTar and J. Kogut, Phys. Rev. Lett. **59**, 399 (1987); Phys. Rev. D **36**, 2828 (1987); T. A. DeGrand and C. E. DeTar, Phys. Rev. D **34**, 2469 (1986).

[5] F. R. Brown, F. P. Bulter, H. Chen, N. H. Christ, Z. Dong, W. Schaffer, L. I. Unger, and A. Vaccarino, Phys. Rev. Lett. **65**, 2491 (1990); M. Fukugita, H. Mino, M. Okawa, and A. Ukawa, *ibid.* **65**, 816 (1990); P. F. Hsieh, Phys. Rev. D **43**, 3475 (1991).

[6] V. D. Barger and R. J. N. Phillips, *Collider Physics* (Addison-Wesley, New York, 1987), and references therein; P. D. B. Collins and A. D. Martin, *Hadron Interactions* (Adam Hilger, Bristol, 1984).

[7] G. Altarelli, Phys. Rep. **81**, 1 (1982).

[8] F. E. Close, *An Introduction to Quarks and Partons* (Academic, London, 1979).

[9] P. Levai and B. Müller, Duke Report No. Duke-Th-90-10, 1991 (submitted to Phys. Lett. B).

[10] S. Mandelstam, Phys. Rep. **13C**, 261 (1974); J. Scherk, Rev. Mod. Phys. **47**, 123 (1975).

[11] S. Ohta, M. Fukugita, and A. Ukawa, Phys. Lett. **B173**, 15 (1986); J. Wosiek and R. W. Haymaker, Phys. Rev. D **36**, 3297 (1987).

[12] M. Baker, J. S. Ball, and F. Zachariasen, Phys. Rev. D **37**, 1036 (1988).

[13] J. Kogut and L. Susskind, Phys. Rev. D **11**, 395 (1975); N. Isgur and J. Patton, *ibid.* **31**, 2910 (1985); G. A. Miller, *ibid.* **37**, 2431 (1988).

[14] G. A. Miller, Nucl. Phys. **A497**, 277c (1989).

[15] D. Robson, Phys. Rev. D **35**, 907 (1987).

[16] A. K. Kerman, T. Matsui, and B. Svetitsky, Phys. Rev. Lett. **56**, 219 (1986); G. Gatoff, A. K. Kerman, and T. Matsui, Phys. Rev. D **36**, 114 (1987).

[17] J. Knoll, Z. Phys. C **38**, 187 (1988).

[18] R. Kokoski and N. Isgur, Phys. Rev. D **35**, 907 (1987); G. A. Miller, *ibid.* **37**, 2431 (1988); P. Geiger and N. Isgur, *ibid.* **41**, 1595 (1990).

[19] P. Mättig, Phys. Rep. **177**, 141 (1989).

[20] K. Sailer, B. Müller, and W. Greiner, J. Mod. Phys. **A4**, 437 (1989); K. Sailer, B. Müller, and W. Greiner, in *The Nuclear Equation of State*, Proceedings, edited by W. Greiner and H. Stocker (Plenum, New York, 1990), p.531.

[21] E. A. Remler, Proceedings of the XXXI Cracow School of Theoretical Physics, Zakopane, Poland, 1991 (unpublished); E. A. Remler, Proceedings of the International Workshop on Quark-Gluon Structure of Hadrons and Nuclei, Shanghai, 1990 (unpublished); E. A. Remler, College of William & Mary Report, 1988 (unpublished); E. A. Remler, Gross Properties of Nuclei and Nuclear Excitations, Proceedings, Hirschegg, 1987 (unpublished), p.24.

[22] S. M. Berman, J. D. Bjorken, and J. B. Kogut, Phys. Rev. D **4**, 3388 (1971); R. F. Cahalan, K. A. Geer, J. Kogut, and L. Suskind, *ibid.* **11**, 1199 (1975); B. L. Combridge, J. Kripfganz, and J. Ranft, Phys. Lett. **70B**, 234 (1977); R. Cutler and D. Sivers, Phys. Rev. D **17**, 196 (1978).

[23] J. P. Blaizot and A. H. Mueller, Nucl. Phys. **B289**, 847 (1987).

[24] K. Kajantie, P. V. Landshoff, and J. Lindfors, Phys. Rev. Lett. **59**, 2527 (1987).

[25] N. Isgur, Nucl. Phys. **A497**, 91c (1989); K. Maltman and N. Isgur, Phys. Rev. D **29**, 952 (1984).

[26] P. J. Mulders and A. E. L. Dieperink, Nucl. Phys. **A483**, 461 (1988); A. H. Mueller, *ibid.* **A498**, 41c (1989).

[27] R. Anishetty, P. Koehler, and L. McLerran, Phys. Rev. D **22**, 2793 (1980).

[28] B. Andersson and G. Gustafson, Z. Phys. C **3**, 223 (1980); B. Andersson, G. Gustafson, G. Ingelman, and T. Sjostrand, Phys. Rep. **97**, 33 (1983).

[29] B. Andersson, G. Gustafson, and B. Nilsson-Almqvist, Nucl. Phys. **B281**, 289 (1987).

[30] K. Werner, Z. Phys. C **42**, 85 (1989).

[31] J. Ranft, Phys. Rev. D **37**, 1842 (1988).

[32] X. Artru and G. Mennessier, Nucl. Phys. **B70**, 93 (1974);

X. Artru, *ibid.* **B85**, 442 (1975); X. Artru, Phys. Rep. **97**, 147 (1983).
[33] T. Gotō, Prog. Theor. Phys. **46**, 1560 (1971); P. Goddard, J. Goldstone, C. Rebbi, and C. B. Thorn, Nucl. Phys. **B56**, 109 (1973).
[34] D. J. Dean, Ph.D. Thesis, Vanderbilt University, 1991.
[35] P. D. B. Collins, *Regge Theory and High Energy Physics* (Cambridge University Press, Cambridge, England, 1977).
[36] R. D. Field and R. P. Feynman, Nucl. Phys. **B136**, 1 (1978).
[37] M. G. Bowler, Z. Phys. C **22**, 155 (1984).
[38] B. Andersson, G. Gustafson, and B. Söderberg, Z. Phys. C **20**, 317 (1983).
[39] N. K. Glendenning and T. Matsui, Phys. Rev. D **28**, 2890 (1983).
[40] T. Fujita and J. Hüfner, Phys. Rev. D **37**, 604 (1989); C. Wong, R. Wang, and C. Shih, *ibid.* **44**, 257 (1991).
[41] J. Schwinger, Phys. Rev. **82**, 664 (1951); J. Schwinger, *ibid.* **128**, 2425 (1962); A. Casher, H. Newberger, and S. Nussinov, Phys. Rev. D **20**, 179 (1979).
[42] J. D. Bjorken, Phys. Rev. D **27**, 140 (1983).
[43] K. Sailer, Th. Schönfeld, A. Schäfer, B. Müller, and W. Greiner, University of Frankfurt Report No. UFTP 244/1990.
[44] M. Althoff *et al.*, TASSO Collaboration, Z. Phys. C **22**, 307 (1984); R. Brandelik *et al.*, TASSO Collaboration, Phys. Lett. **170B**, 290 (1981).
[45] P. Kesten *et al.*, Phys. Lett. **161B**, 412 (1985).
[46] T. Sloan, G. Smadja, and R. Voss, Phys. Rep. **162**, 45 (1988).
[47] D. H. Perkins, *Introduction to High Energy Physics*, 3rd edition (Addison-Wesley, Reading, MA, 1987).
[48] E. Eichten, I. Hinchliffe, K. Lane, and C. Quigg, Rev. Mod. Phys. **56**, 579 (1984); A. D. Martin, R. G. Roberts, and W. J. Stirling, Phys. Rev. D **37**, 1161 (1988).
[49] A. Bodek *et al.*, Phys. Rev. D **20**, 1471 (1979).
[50] K. Werner, Phys. Rev. Lett. **62**, 2460 (1989).
[51] L. Magnea and G. Sterman, *Proceedings of the Workshop on Hadron Structure Functions and Parton Distributions*, edited by D. F. Geesaman, J. Morfin, C. Sazama, and W.K. Tung (World Scientific, Singapore, 1990), p.423.
[52] J.-S. Wu, D. J. Dean, A. S. Umar, and M. R. Strayer (unpublished).
[53] C. Itzykson and J. Zuber, *Quantum Field Theory* (McGraw-Hill, New York, 1980), p. 200.
[54] E. V. Shuryak and A. I. Vainstein, Nucl. Phys. **B199**, 451 (1982).
[55] D. J. Dean, J.-S. Wu, A. S. Umar, and M. R. Strayer (unpublished).
[56] W. Thome *et al.*, Nucl. Phys. **B129**, 365 (1978).
[57] C. De Marzo *et al.*, Phys. Rev. D **26**, 1019 (1982).
[58] A. Breakstone *et al.*, Phys. Lett. **132B**, 458 (1983); Phys. Rev. D **30**, 528 (1984).

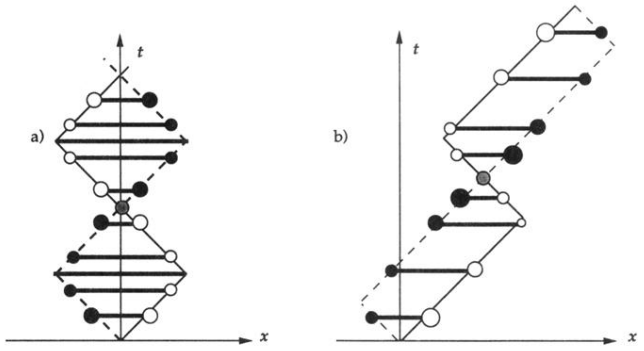

FIG. 3. (a) The motion of a string with end points executing one-dimensional (yo-yo) motion. The solid curve represents the motion of one of the end points and the dashed curve the other. The details are explained in the text. (b) A boosted one-dimensional string is illustrated.